Journal of Catalysis 315 (2014) 6–14

Contents lists available at ScienceDirect

Journal of Catalysis

journal homepage: www.elsevier.com/locate/jcat

Partially oxidized gold nanoparticles: A catalytic base-free system for the aerobic homocoupling of alkynes

Mercedes Boronat [a], Siris Laursen [a,b], Antonio Leyva-Pérez [a], Judit Oliver-Meseguer [a], Diego Combita [a], Avelino Corma [a,*]

[a] Instituto de Tecnología Química, Universidad Politécnica de Valencia, Consejo Superior de Investigaciones Científicas, Av. de los Naranjos, s/n, 46022 Valencia, Spain
[b] Department of Chemical and Biomolecular Engineering, University of Tennessee, Knoxville, TN 37996-2200, USA

ARTICLE INFO

Article history:
Received 20 February 2014
Revised 2 April 2014
Accepted 3 April 2014

Keywords:
Gold
Heterogeneous catalysis
DFT
Oxidative coupling of alkynes
Reaction mechanism
C—H activation

ABSTRACT

The mechanism of alkyne homocoupling over gold nanoparticles and clusters, isolated and supported on CeO_2, has been theoretically investigated by means of periodic DFT calculations. The theoretical study indicates that O_2 dissociation on gold generates basic O atoms able to abstract the proton of the alkyne, and cationic $Au^{\delta+}$ and Au^{+} species that decrease the activation barrier for the C—C bond forming step. Kinetic results show that the base-free homocoupling of alkynes is effectively catalyzed by gold nanoparticles supported on different solids, and confirm the theoretical prediction that the dissociation of oxygen on the gold nanoparticle is the controlling step of the global reaction.

1. Introduction

The synthesis of 1,3-diynes, which are important building blocks in fine chemistry, pharmaceuticals and bioactive compounds, has been traditionally carried out via oxidative homocoupling of terminal alkynes. Copper salts assisted by a base, as well as catalytic systems formed by a combination of palladium and copper salts have been extensively used in homogeneous phase [1–4]. The development of heterogeneous catalysts for the homocoupling of alkynes, with the advantages of easy separation and recycling, is interesting from an economic and environmental points of view, and some examples exist in the literature reporting the catalytic activity of copper-containing hydrotalcites [5,6], zeolites [7,8], and $Cu(OH)_x$ supported on different transition metal oxides [9,10]. It has also been reported that alkyne homocoupling occurs under typical conditions for Sonogashira cross-coupling reactions, both in homogeneous phase using Pd organocatalysts [11,12] and over heterogeneous Au/CeO_2 [13] and Au/La_2O_3 [14] catalysts. We recently investigated the mechanism of the Sonogashira reaction between iodobenzene (IB) and phenylacetylene (PA) on Au/CeO_2 catalysts and found that PA can be activated at cationic gold sites at the metal-support interface, producing a non-negligible amount of diphenyldiacetylene (DPDA), i.e., the product of PA homocoupling [15]. In this work, we combine DFT calculations with kinetic experiments to firstly determine the mechanism of PA homocoupling on heterogeneous gold catalysts and, consequently, to identify the nature of the gold active sites required to prepare an optimized heterogeneous catalyst for the homocoupling of alkynes.

2. Experimental section

2.1. Models and methods

The mechanism of PA homocoupling was investigated by means of periodic density functional theory, using the Perdew–Wang (PW91) exchange–correlation functional within the generalized gradient approach (GGA) [16,17] as implemented in the VASP code [18,19]. The valence density was expanded in a plane wave basis set with a kinetic energy cutoff of 500 eV, and the effect of the core electrons in the valence density was taken into account by means of the projected augmented wave (PAW) formalism [20]. Integration in the reciprocal space was carried out at the Γ k-point of the Brillouin zone. Transition states were located using the DIMER [21,22] and NEB [23] algorithms, and stationary points

* Corresponding author. Fax: +34 9638 77809.
E-mail addresses: boronat@itq.upv.es (M. Boronat), slaursen@utk.edu (S. Laursen), anleyva@itq.upv.es (A. Leyva-Pérez), joliverm@itq.upv.es (J. Oliver-Meseguer), diecmmer@posgrado.upv.es (D. Combita), acorma@itq.upv.es (A. Corma).

http://dx.doi.org/10.1016/j.jcat.2014.04.003
0021-9517/

were characterized by pertinent frequency analysis calculations. Charge distributions were estimated using the theory of atoms in molecules (AIM) of Bader using the algorithm developed by Henkelman [24,25]. In the case of modeling CeO_2, the Hubbard repulsion term (U) with a value of 5 eV was applied to the cerium atoms in all calculations [26].

Neutral gold clusters and nanoparticles were modeled by means of an Au_3 system formed by three gold atoms and by an Au_{38} system having a typical cuboctahedral shape and ~1 nm diameter, respectively. A partially oxidized gold nanoparticle was obtained by adding 16 O atoms to the surface of the Au_{38} system, generating a $Au_{38}O_{16}$ model previously described [27]. These models were placed in a $25 \times 25 \times 25$ Å^3 cubic box, large enough as to avoid interactions between periodically repeated nanoparticles or adsorbates, and during the geometry optimizations, only the positions of the adsorbates and of the O atoms directly involved in the mechanism were allowed to fully relax.

A stoichiometric CeO_2 (1 1 1) surface was modeled by means of a (4×3) supercell slab containing 64 O atoms and 32 Ce atoms, and then, four different models were generated to simulate Au nanoparticles supported on CeO_2: (a) *AuO_x/CeO_2* model: a two atomic layer thick Au nano-rod containing 20 Au atoms was placed on the stoichiometric CeO_2 (1 1 1) surface and six additional oxygen atoms were added between the Au nano-rod and the CeO_2 surface Ce^{4+} sites. This model contains both metallic Au^0 and cationic $Au^{\delta+}$ species at the metal–support interface. (b) *Au_2O_3/CeO_2* model: a gold oxide strip consisting of 6 Au atoms and 9 O atoms was placed on the stoichiometric CeO_2 (1 1 1) surface, generating a system containing cationic Au^+ and Au^{3+} atoms. (c) *Au_{10}/CeO_2* model: a small cluster consisting of ten Au atoms arranged in two layers having 7 and 3 Au atoms, respectively, was placed on the stoichiometric CeO_2 (1 1 1) surface, resulting in a supported Au nanoparticle containing metallic low coordinated Au^0 atoms, and (d) *Au_9O_7/CeO_2* model: a small cluster consisting of nine Au atoms was placed on the stoichiometric CeO_2 (1 1 1) surface, and 7 O atoms were added at the metal-support interface, generating a system containing three low-coordinated metallic Au^0 atoms on top of the particle and four cationic Au^+ sites at the metal-support interface. To obtain the optimized structures of these models, the Ce and O atoms in the bottom layer of each system were kept fixed in their bulk optimized positions, while the atomic positions of the rest of the atoms were fully relaxed. In the study of the mechanism of PA homocoupling, only the positions of the adsorbates and of the O atoms directly involved in the mechanism were allowed to fully relax during the geometry optimizations.

2.2. Experimental

2.2.1. Catalyst screening and scope

The solid catalyst (Au/Carbon and Au/CeO_2: 41 mg; Au/TiO_2, Au/ZnO, Au/Al_2O_3 and Au/Fe_2O_3: 65 mg, 2 mol% Au) was placed in a thick double-walled 2.5-ml glass reactor equipped with a magnetic stirrer. Then 1,3-dichlorobenzene (0.5 ml) and the corresponding alkyne (0.25 mmol) were added and the vial capped with the pressure system. Molecular oxygen gas was loaded through a needle until the manometer indicated c.a. 5 bars (0.75 mmol). Then, the reactor was placed stirred in a pre-heated oil bath at 170 °C and magnetically stirred for 18 h. After this time, the reactor was cooled with water and the gas released. Diethyl ether (1 ml) was added and the mixture was filtered and submitted to GC and GC–MS analysis after dodecane (22 μl, 0.1 mmol) was added as external standard.

2.2.2. Initial rate measurements

Initial rates were calculated from the slope of the first-order kinetic curves of the homocoupling of *ortho*-tolylacetylene under different pressures of oxygen or at different concentrations of alkyne. The points of the kinetic curves were obtained from independent batch experiments by stopping the reaction at different reaction times. For that, the solid catalyst (Au/C or Au/CeO_2: 41 mg, Au/ZnO: 65 mg; 2 mol% Au) was placed in a thick double-walled 2.5-ml glass reactor equipped with a magnetic stirrer. Then, 1,3-dichlorobenzene (0.5 ml) and the corresponding amount of *ortho*-tolylacetylene were added and the vial capped with the pressure system. Neat molecular oxygen gas was loaded through a needle until the manometer indicated the corresponding pressure. Then, the reactor was magnetically stirred in a pre-heated oil bath at 170 °C for the desired time. After this time, the reactor was cooled with water and the gas released. Diethyl ether (1 ml) was added and the whole mixture was filtered and submitted to GC and GC–MS analysis after dodecane (22 μl, 0.1 mmol) was added as an external standard. The yield of homocoupling of *ortho*-tolylacetylene was plotted versus time and the slope at low yields gives the initial rate in h^{-1}.

2.2.3. Leaching studies

Experiments were carried out following the procedure above detailed but at different reaction times. After representing these data in a plot-time yield graphics, a second set of experiments was carried out as follows: at c.a. 25% conversion, the gas was released and the solid catalyst was filtered at the reaction temperature collecting the filtrates in a second reactor equipped with a magnetic bar. This reactor was closed and placed under the same magnetically stirred bath oil at 170 °C after oxygen atmosphere was re-loaded (0.75 mmol). This protocol was followed for each data point. After the desired time, diethyl ether (1 ml) was added and the mixture was filtered and submitted to GC and GC–MS analysis after dodecane (5.6 μl, 0.025 mmol) was added as external standard. Comparison among the curves gives estimation about the presence of catalytically active species in solution. The results obtained for the batch reactions are similar to those corresponding to single reactions in which aliquots were periodically taken after release of the oxygen atmosphere and re-load.

2.2.4. Reusability studies

Experiments were carried out following the procedure above detailed but recovering the solid catalyst by decantation instead of filtration after diethyl ether (1 ml) addition. The solid was then washed three times with diethyl ether (1 ml), dried, and used in a second run.

3. Results and discussion

3.1. Theoretical study of reaction mechanism on gold catalyst models

In a first step, we investigated the mechanism of PA homocoupling on a small Au_3 cluster and on two different models of isolated gold nanoparticles, that is, a Au_{38} system containing only metallic low coordinated Au^0 sites (see Table 1), and a

Table 1
Calculated Bader charges on selected Au atoms in different gold catalyst models.

Model	Au^0	$Au^{\delta+}$	Au^+	Au^{3+}
Au_3	~0	–	–	–
Au_{38}	~0	–	–	–
Au_2O, Au_2O_3	–	–	0.47	1.19
$Au_{38}O_{16}$	~0	0.21	0.47	–
AuO_x/CeO_2	~0	0.33	0.65	
Au_2O_3/CeO_2			~0.76	~1.14
Au_{10}/CeO_2	~0			
Au_9O_7/CeO_2	~0		~0.64	

partially oxidized gold nanoparticle containing three types of sites: metallic Au^0 centers, slightly positively charged $Au^{\delta+}$ sites directly bonded to one O atom, and cationic Au^+ centers in which the Au atom is directly bonded to two O atoms forming a linear O—Au—O structure, as described in previous work [27]. The calculated adsorption, activation and reaction energies, schematized in Fig. 1, are summarized in Table 2 and the optimized geometries of the structures involved in the mechanism are depicted in Figs. 2–4.

PA adsorption and dissociation on isolated neutral gold nanoparticles was investigated as one of the elementary steps in the Sonogashira reaction between PA and IB [15]. It was found that PA adsorbs strongly on low coordinated neutral Au^0 atoms at corner or edge sites, but the dissociation process is endothermic by 20 kcal/mol and involves an activation energy of almost 40 kcal/mol (see Table 2). As previously described, the presence of a base (carbonate) lowers the barrier to 9.0 kcal/mol, and the process becomes exothermic by 7.7 kcal/mol. After dissociation on an isolated Au_{38} nanoparticle, the phenylacetylenyl fragment is placed on top of a low coordinated Au atom, while the H atom occupies a bridge position between two Au atoms (see Fig. 2). The surface coupling step occurs through a transition state in which the C—C bond is formed while the two organic fragments are still quite strongly bonded to the Au atoms, as indicated by the optimized values of the C—Au distances, 2.04 Å. The calculated activation energy for this elementary step is 25 kcal/mol and DPDA formation and desorption releases 8.5 kcal/mol.

It has been recently reported that small gold clusters are highly efficient in the activation of the C≡C bond in alkynes [28,29] and, in order to check the relevance of this effect on the mechanism of alkyne homocoupling, PA adsorption and dissociation over a small Au_3 cluster was also investigated. As depicted in Fig. 3, PA interacts strongly with the low coordinated atoms of the Au_3 cluster producing an activation and weakening of the C≡C bond reflected in an increase in the CC bond length of 0.05 Å. However, this interaction does not favor the desired dissociation of the C—H bond, which is endothermic by 21 kcal/mol and involves an activation barrier of 30 kcal/mol. Moreover, the calculated activation energy for the coupling of two phenylacetylenyl fragments attached to the Au_3 cluster is as high as 27.5 kcal/mol, indicating that such small clusters should not be active for alkyne homocoupling.

The effect of cationic gold sites and basic oxygen atoms is more relevant. PA adsorption at slightly positive $Au^{\delta+}$ sites and at cationic Au^+ centers present in the partially oxidized $Au_{38}O_{16}$ model is energetically favored (−7.3 and −4.1 kcal/mol at $Au^{\delta+}$ and Au^+, respectively) and the activation barrier for its deprotonation (14.4 and 12.6 at $Au^{\delta+}$ and Au^+, respectively) is considerably lower than on the pure metallic Au_{38} nanoparticle, because it is assisted by a basic O atom from the gold oxide over layer. After dissociation, the phenylacetylenyl fragment is occupying a bridge position between a Au^0 and a $Au^{\delta+}$ (or Au^+) site (see Fig. 4). The

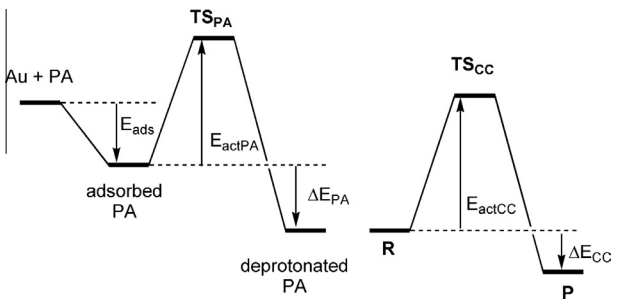

Fig. 1. Schematic representation of energy profiles for PA dissociation (left) and for bimolecular coupling step (right) in gold catalyzed PA homocoupling.

calculated reaction energy for PA deprotonation, 10.8 kcal/mol, is not as endothermic as on the Au_{38} model, but we should take into account that it also includes the energy gain due to formation of a O—H bond. To compare the stability of phenylacetylenyl fragments directly bonded to metallic or cationic Au sites, a $Au_{38}O_2$ model was used that contains metallic Au^0 and cationic $Au^{\delta+}$ and Au^+ sites (see Fig. 5 and Table 1). Phenylacetylenyl interacts much stronger with metallic Au^0 atoms in Au_{38} and $Au_{38}O_2$ models than with cationic $Au^{\delta+}$ centers and Au^+ sites, following the linear trend depicted in Fig. 5. This result suggests a higher reactivity of phenylacetylenyl fragments bonded to cationic $Au^{\delta+}$ and Au^+ sites and, indeed, the calculated activation energies for the surface coupling step are in this line. The barrier obtained on the $Au_{38}O_{16}$ model, in which the two reactant phenylacetylenyl fragments are directly interacting with cationic $Au^{\delta+}$ sites, is 18 kcal/mol, 7 kcal/mol lower than on the metallic Au_{38} system.

Besides PA deprotonation and surface coupling steps, O_2 dissociation generating adsorbed O atoms and cationic $Au^{\delta+}$ and Au^+ sites is necessary to close the catalytic cycle. It should be remarked at this point that the activation barriers for O_2 dissociation over gold nanoparticles vary considerably with particle size and shape [27,30,31]. Thus, for instance, the activation barriers for successive O_2 dissociation over the most favorable site of cuboctahedral Au_{38} NPs leading to formation of a gold oxide over layer are around 8 kcal/mol or less [27]. But when the process takes place at edge sites also present in Au_{38} and in larger, smaller or irregular gold nanoparticles, the activation barriers increase by 10–20 kcal/mol [30,31], suggesting that O_2 dissociation might be the rate determining step for the global homocoupling reaction.

Next, we considered four different models for the Au/CeO_2 catalysts containing different types of neutral and cationic sites: (a) a gold nanorod on a partially oxidized $CeO_2(111)$ surface (AuO_x/CeO_2 model, see Computational Details section) that contains both Au^0 and $Au^{\delta+}$ species; (b) a Au_2O_3 strip on stoichiometric $CeO_2(111)$ that only contains cationic Au^+ and Au^{3+} atoms (Au_2O_3/CeO_2 model); (c) a Au_{10} cluster on stoichiometric $CeO_2(111)$ that only contains metallic low coordinated Au^0 sites (Au_{10}/CeO_2 model); and (d) a Au_9 cluster on a partially oxidized $CeO_2(111)$ surface (Au_9O_7/CeO_2 model) that contains low coordinated metallic Au^0 and cationic Au^+ species, as indicated by the Bader charges listed in Table 1.

PA was initially adsorbed at neutral Au^0 and cationic $Au^{\delta+}$, Au^+ and Au^{3+} atoms present in the different Au/CeO_2 models, and the resulting optimized structures and calculated adsorption energies are given in Fig. 6 and Table 2, respectively. It was found that PA cannot adsorb on cationic Au^{3+} atoms present in the Au_2O_3/CeO_2 model, but interacts with Au^+ sites in the same system, with calculated adsorption energies ranging between −6.7 and −9.5 kcal/mol. A weaker interaction was found with slightly positive $Au^{\delta+}$ sites present in AuO_x/CeO_2 and Au_9O_7/CeO_2 models, with calculated adsorption energies around −3 kcal/mol. And, as found for isolated gold nanoparticles, the stronger interaction is obtained for PA adsorption at low coordinated metallic Au^0 sites present in Au_{10}/CeO_2 and Au_9O_7/CeO_2 models, with calculated adsorption energies ranging between −9 and −13 kcal/mol.

PA dissociation on metallic Au^0 sites was not investigated on Au/CeO_2 models based on the high activation barrier obtained on the isolated Au_{38} nanoparticle, but was calculated on all cationic Au sites. In all cases, the activation energies obtained were lower than 15 kcal/mol, and the dissociation process was found to be exothermic. However, it is not possible to directly compare the stability of the phenylacetylenyl fragments from calculated ΔE_{PA} reaction energies on the different models because the dissociation process always involves formation of a O—H bond whose stability depends on the basicity of the O atom involved. To avoid this problem in the calculation of the activation barriers for the bimolecular

Table 2
Adsorption, activation and reaction energies (in kcal/mol) calculated for the elementary steps schematized in Fig. 1 on neutral Au^0 and cationic $Au^{\delta+}$ and Au^+ sites on different gold catalyst models.

Model	Au site	$E_{ads\ PA}$	$E_{act\ PA}$	$E_{act\ CC}$
Au_3	Au^0	−37.0	30.0	27.5
Au_{38}	Au^0	−14.8	39.9	25.0
$Au_{38}O_{16}$	$Au^{\delta+}$	−7.3	14.4	18.0
$Au_{38}O_{16}$	Au^+	−4.1	12.6	12.4
AuO_x/CeO_2	$Au^{\delta+}$	−2.7	8.7	38.3
Au_2O_3/CeO_2	Au^+	−9.5	9.7	16.1
Au_{10}/CeO_2	Au^0	−9.0		33.0
Au_9O_7/CeO_2	Au^0	−12.5		
Au_9O_7/CeO_2	Au^+	−3.5	18.2	2.5

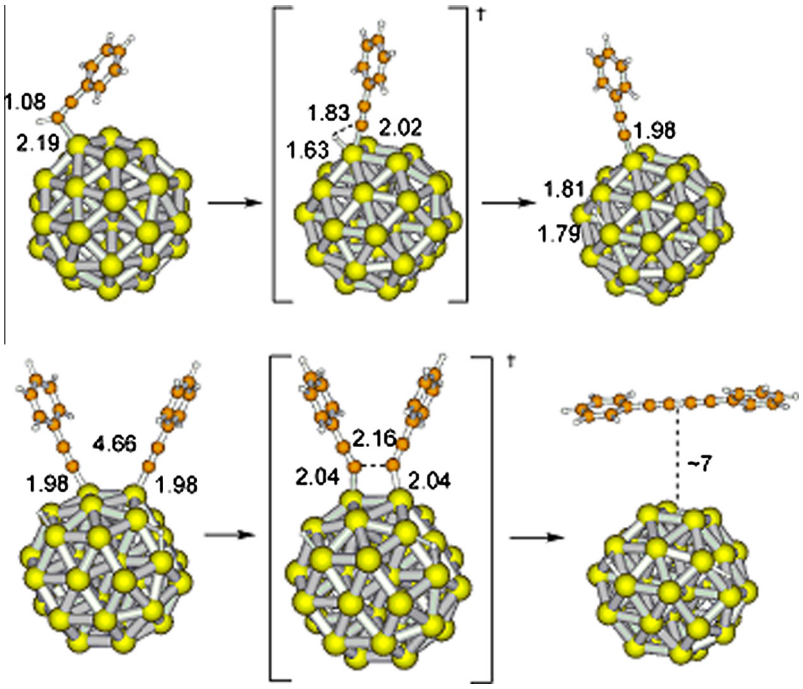

Fig. 2. Optimized geometries of the species involved in the mechanism of PA homocoupling on an isolated neutral Au_{38} nanoparticle. Distances in Å.

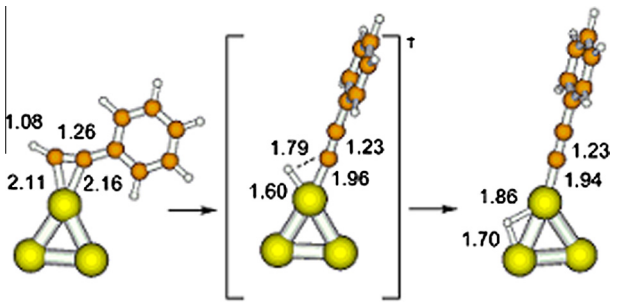

Fig. 3. Optimized geometries of the species involved in the mechanism of PA activation on an isolated neutral Au_3 cluster. Distances in Å.

surface coupling step, the H atoms resulting from PA dissociation were placed in all cases on the CeO_2 support, so that the stabilization due to formation of this bond is equivalent in all systems. The optimized geometries of the reactants and transition states for the surface coupling step on the four different Au/CeO_2 models considered are depicted in Fig. 7, and the calculated activation energies are listed in Table 2. In all transition states, the two carbon atoms involved in the formation of the new C—C bond are still strongly attached to the Au atoms, and the distance between them is ~2.2 Å. But this similarity in the optimized geometries is not reflected in the calculated activation energies. The highest $E_{act\ CC}$ values are obtained on the AuO_x/CeO_2 and Au_{10}/CeO_2 models, 38 and 33 kcal/mol, respectively, and the reason is that the phenylacetylenyl fragments are in both cases initially coordinated to three metallic Au^0 atoms, which is the most stable situation as shown in Fig. 5. When the phenylacetylenyl fragments are initially attached to cationic Au^+ sites in the Au_2O_3/CeO_2 model, the activation energy is considerably lower, 16.1 kcal/mol. And the most favorable situation is found on the Au_9O_7/CeO_2 model. In this case, not only the reactants are less stable because they are bonded to cationic Au^+ sites, but there is also an extra stabilization in the transition state due to formation of a new Au—C bond (see Fig. 7d, right). As a result, the calculated activation energy is only 2.5 kcal/mol.

O_2 dissociation generating adsorbed O atoms and cationic gold sites in supported gold catalysts has been widely studied in the literature, mainly in relation to the mechanism of low temperature CO oxidation [32–35]. Despite the large variety of models and methods employed, there is general consensus that molecular O_2 preferentially adsorbs at the interface between the gold

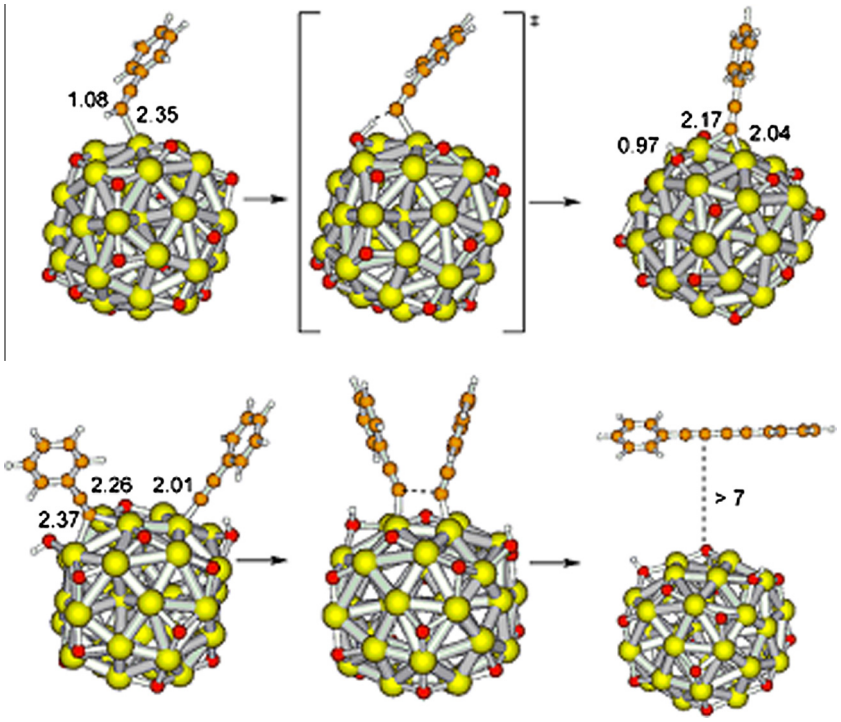

Fig. 4. Optimized geometries of the species involved in the mechanism of PA homocoupling on an isolated partially oxidized $Au_{38}O_{16}$ nanoparticle. Distances in Å.

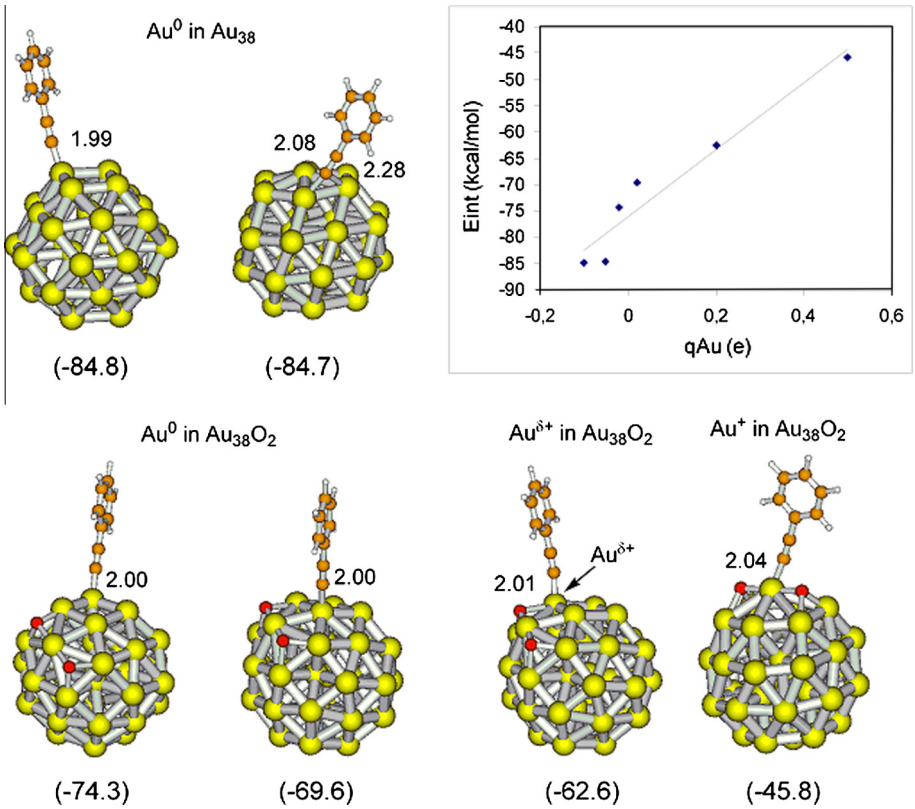

Fig. 5. Interaction of phenylacetylenyl radical with different metallic Au^0 and cationic $Au^{\delta+}$ and Au^+ sites on isolated Au nanoparticles, and relationship between calculated interaction energies (values in brackets, in kcal/mol) and net atomic charge on Au atom. Distances in Å.

nanoparticle and the metal oxide support, and that the presence of either O vacancy defects in reduced surfaces or extra O atoms in oxidized surfaces enhances reactivity by decreasing the activation barriers for O_2 dissociation[36,37].

It can be concluded from the theoretical study that PA adsorbs at metallic Au^0 and cationic $Au^{\delta+}$ and Au^+ sites, and that its deprotonation is energetically feasible in all systems having O atoms able to abstract the proton, suggesting that a base might not be

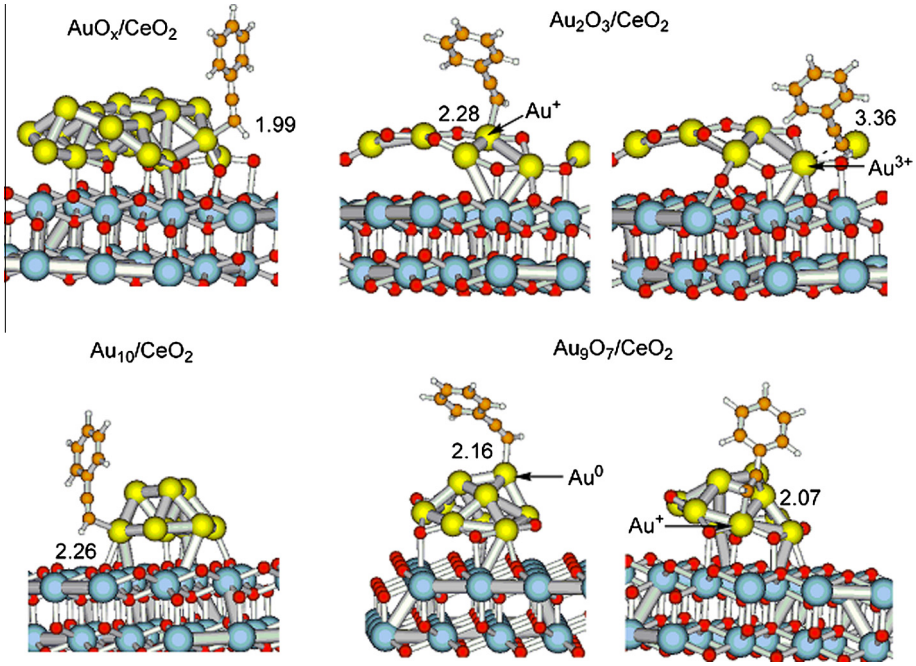

Fig. 6. PA adsorption at neutral and cationic Au sites in different Au/CeO_2 models.

necessary to perform the homocoupling PA provided that the gold nanoparticles are partially oxidized. The phenylacetylenyl fragments directly attached to cationic Au species are less stable and consequently more reactive than those bonded to metallic Au^0 atoms and, as a consequence, the activation barriers for the bimolecular surface coupling step are lower on the catalysts containing cationic gold. Finally, in the absence of a base, the protons that are transferred from PA to the oxygen atoms at the metal-support interface will form H_2O that will desorb from the catalyst, decreasing the concentration of cationic $Au^{\delta+}$ and Au^+ active sites, which should be regenerated by reaction with O_2.

A remarkable conclusion from this part of the study is the double role of O_2 on the reaction mechanism. On one hand, O_2 is the final acceptor of electrons and protons generated in the dissociation of the C—H bond of PA. But on the other hand, its dissociation is necessary to generate the cationic $Au^{\delta+}$ and Au^+ active sites on the surface of isolated gold nanoparticles or at the gold-support interface in Au/CeO_2 catalysts. As previously discussed, the activation energy for O_2 dissociation depends on the size and shape of the gold nanoparticles and the interaction with the support, and might become the rate determining step of the global process. In particular, it suggests that small gold clusters that are able to efficiently activate the alkyne C≡C bond but cannot dissociate molecular O_2 [29], will probably be inactive toward alkyne homocoupling.

3.2. Catalytic activity of supported gold nanoparticles

According to the theoretical study, homocoupling of alkynes in the presence of O_2 should be effectively catalyzed by gold nanoparticles without the need of an added base, provided that these gold nanoparticles are able to dissociate molecular O_2 and become partially oxidized, generating basic O atoms able to abstract the proton from the alkyne as well as cationic $Au^{\delta+}$ and Au^+ sites that favor the C—C bond forming step.

To test the above hypothesis, we carried out the homocoupling of *ortho*-tolylacetylene in the presence of O_2 and in absence of any base on a series of supported gold catalysts, including Au/CeO_2, Au/C, Au/TiO_2, Au/ZnO, Au/Al_2O_3 and Au/Fe_2O_3. All of them are able to stabilize surface $Au^{\delta+}$ species. As shown in Fig. 8, good catalytic activities were found with all materials. To confirm that the catalysis was heterogeneous, the reaction was stopped after ~20% conversion and the solid catalyst was filtered in hot. Although some gold was leached out from Au/CeO_2, Au/C and Au/Fe_2O_3 (1.0%, 0.1% and 0.2% of the initial gold, respectively), the gold species in solution gave only a marginal activity in the presence of air (see Figs. S1–S3), which is consistent with the fact that when AuCl or $AuNaCl_4$ were introduced as catalyst in solution, no activity was observed. The scope of the homocoupling reaction under O_2-promoted base-free conditions was examined for different alkynes in the presence of catalytic amounts of Au/C (see Table 3). Aromatic (entries 1–9) and aliphatic alkynes (entries 10–11) can be both coupled with yields ranging from 60% to 90%. These yields are good, taking into consideration that alkynes can undergo other reactions in the presence of supported gold catalysts [38]. The reusability of the Au—C catalyst was also tested and complete conversion and selectivity for the homocoupling product was obtained after four uses (entry 2).

At this point, it is confirmed that the coupling of alkynes is catalyzed by gold nanoparticles in the absence of a base. The second proposal from the theoretical part of the work is that O_2 dissociation on the gold nanoparticles generating the oxidized $Au^{\delta+}$ and Au^+ active sites is, most probably, the rate determining step of the global reaction. To confirm this hypothesis, the influence of O_2 pressure on the initial reaction rate was investigated. As shown in Fig. 9 for Au/CeO_2, Au/C and Au/ZnO, the reaction practically does not occur under N_2 atmosphere, while a maximum in activity is obtained at intermediate O_2 pressures (between 2 and 3 equivalents of O_2, depending on the catalyst), and further increasing O_2 pressure suppresses activity. On the other hand, no influence of the alkyne concentration on the reaction rate is observed in the range studied. The above results lead to the conclusion that the controlling step during the alkyne coupling on gold nanoparticles under our reaction conditions is the dissociation of oxygen generating the cationic $Au^{\delta+}$ and Au^+ active sites. To further clarify whether the decrease in catalytic activity observed at high O_2 pressure is due to competitive adsorption of reactants or involves

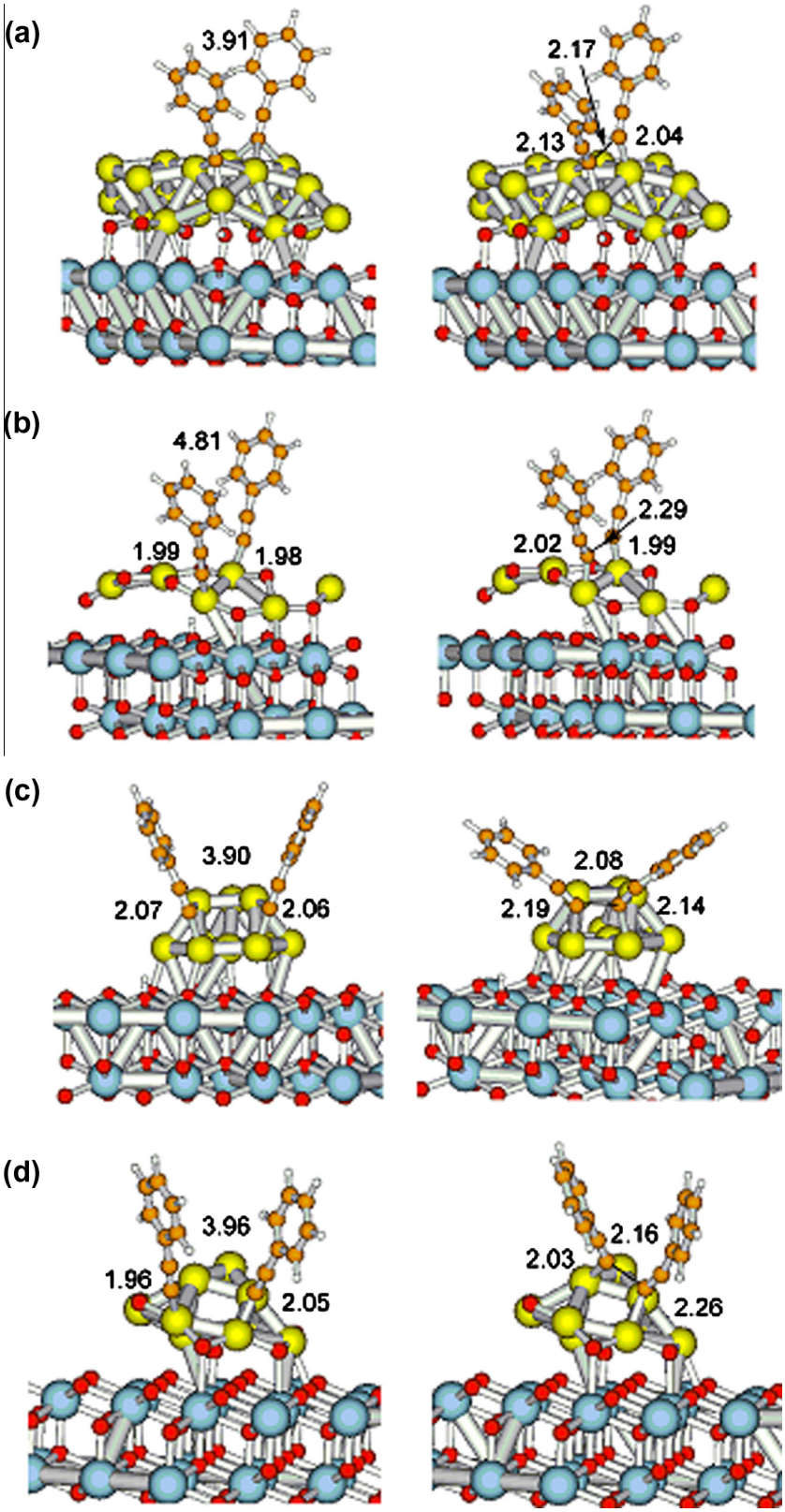

Fig. 7. Optimized structures of reactants (left) and transition states (right) involved in the bimolecular surface coupling step on (a) Au/ox-CeO_2, (b) Au_2O_3/CeO_2, (c) Au_{10}/CeO_2 and (d) Au_9/ox-CeO_2 models. Distances in Å.

an irreversible modification of the catalyst, a sample of Au/ZnO that had been used at 6 bar O_2 pressure and found to be inactive was reused at 2 bar O_2 pressure. Under these new conditions, it showed the same activity that the as-prepared Au/ZnO samples, indicating that the catalyst did not undergo any irreversible deactivation or transformation under reaction conditions. Moreover,

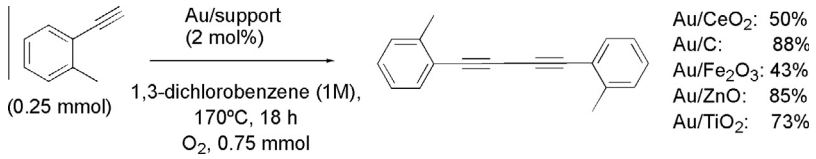

Fig. 8. Base-free Au-supported-catalyzed oxidative homocoupling of *ortho*-tolylacetylene. GC yields.

Table 3
Results for the base-free oxidative homocoupling of alkynes catalyzed by Au—C under an oxygen atmosphere.

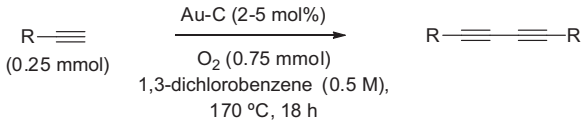

Run	*R*	Catalyst (mol%)	Yield (%)[a]
1	H	2	70
2	*o*-Tolyl	2	85[b]
3	*o*-Tolyl	5	90[c]
4	*m*-Tolyl	5	80
5	*o*-Chlorophenyl	2	85
6	*m*-Chlorophenyl	2	77
7	*o*-Bromophenyl	5	67
8	*m*-Bromophenyl	5	80
9	*m*-Anisyl	2	65
10	Decyl	2	60
11	Dodecyl	2	65

[a] GC yield, products isolated by column chromatography after reaction.
[b] After 4 uses the yield is similar (81%).
[c] Conventional glassware, fitted with a septum rubber and coupled to an O_2 balloon.

DFT adsorption energy values obtained for PA and O_2 interaction with a Au_{38} nanoparticle are −14.8 kcal/mol (Table 2) and −20 kcal/mol [31] respectively, suggesting the possibility of competitive adsorption at the active sites.

The results obtained suggest that the alkyne homocoupling reaction should only occur on those gold particles able to dissociate oxygen and to form the "partially oxidized" species. If this is so, then gold clusters with few gold atoms should not be active since it has been shown [29] that they are not able to dissociate oxygen. Indeed, when the homocoupling reaction was carried out under oxygen in a solution containing gold clusters with 3–9 atoms prepared as described in the literature [39,40], no conversion was found (see Fig. S4), in agreement with the predictions made by the theoretical calculations.

4. Conclusion

The mechanism of alkyne homocoupling over gold nanoparticles and clusters, isolated and supported on CeO_2, has been theoretically investigated by means of periodic DFT calculations. Phenylacetylene adsorbs at metallic Au^0 and cationic $Au^{\delta+}$ and Au^+ sites, and its deprotonation is energetically feasible in all systems having basic O atoms able to abstract the proton. On the other

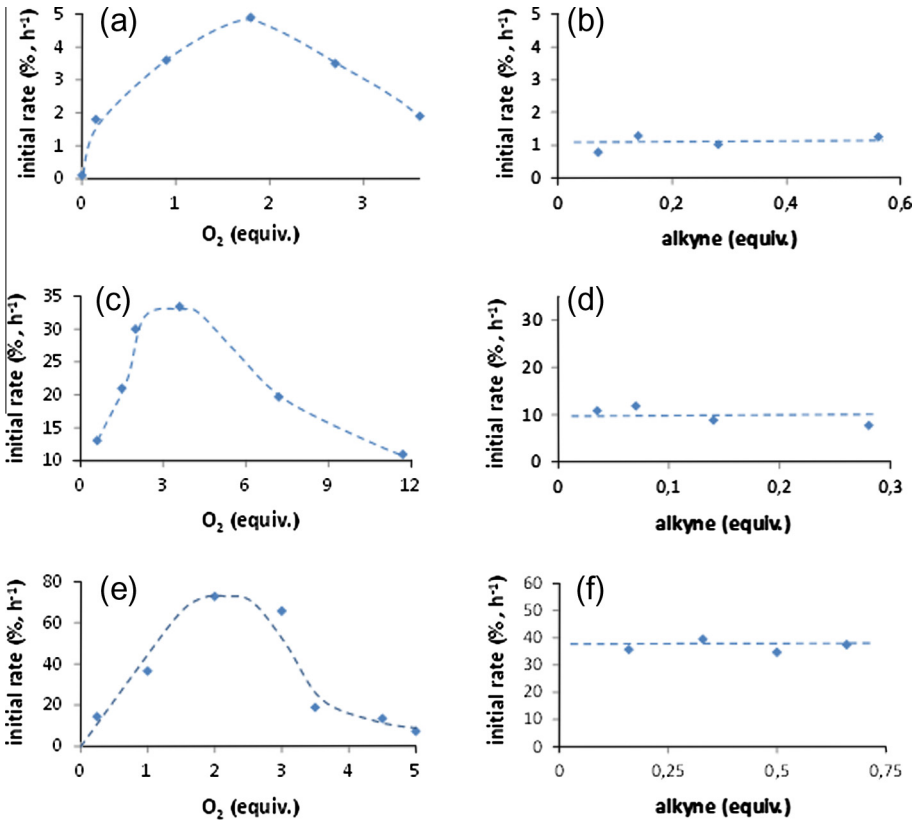

Fig. 9. Dependence of the initial rate *vs.* oxygen and alkyne concentration for Au/CeO_2 (a and b), Au/C (c and d), and Au/ZnO (e and f) for the base-free Au-catalyzed oxidative homocoupling of *ortho*-tolylacetylene. For reaction conditions see Fig. 8 GC yields.

hand, the alkynyl fragments directly attached to cationic $Au^{\delta+}$ and Au^{+} species are more reactive than those bonded to metallic Au^{0} atoms, and as a consequence, the activation barriers for the bimolecular surface coupling step are lower on the catalysts containing cationic gold.

Experimental results show that the base-free homocoupling of different alkynes is catalyzed by gold nanoparticles supported on a large variety of solids, and confirm the theoretical prediction that the dissociation of oxygen on the gold nanoparticle is the controlling step of the global reaction. The easy recovering of the catalyst, the use of air as terminal oxidant, the generation of water as only by-product, and the isolation of the homocoupling products after simple solvent removal makes this C—H activation gold-catalyzed system an extremely practical and environmentally friendly process.

Acknowledgements

Financial support from Spanish MCIINN (Consolider Ingenio 2010-MULTICAT CSD2009-00050 and Subprograma de apoyo a Centros y Universidades de Excelencia Severo Ochoa SEV 2012 0267 Projects) is acknowledged. Red Española de Supercomputación (RES) and Centre de Càlcul de la Universitat de València are gratefully acknowledged for computational facilities and technical assistance. A.L.-P. and J.O.-M. also thank ITQ for a contract.

Appendix A. Supplementary material

Supplementary data associated with this article can be found, in the online version, at http://dx.doi.org/10.1016/j.jcat.2014.04.003.

References

[1] J. Liu, J.W.Y. Lam, B.Z. Tang, Chem. Rev. 109 (2009) 5799.
[2] R.E. Martin, F. Diederich, Angew. Chem. Int. Ed. 38 (1999) 1350.
[3] P. Siemens, R.C. Livingston, F. Diederich, Angew. Chem. Int. Ed. 39 (2000) 2632.
[4] E. Negishi, A. Alimardanov, in: E. Negishi (Ed.), Handbook of Organopalladium Chemistry for Organic Synthesis, Wiley, NewYork, 2002, p. 989.
[5] S.M. Auer, M. Schneider, A. Baiker, J. Chem. Soc. Chem. Commun. (1995) 2057.
[6] B.C. Zhu, X.Z. Jiang, Appl. Organomet. Chem. 21 (2007) 345.
[7] P. Kuhn, A. Alix, M. Kumarraja, B. Louis, P. Pale, J. Sommer, Eur. J. Org. Chem. (2009) 423.
[8] P. Kuhn, P. Pale, J. Sommer, B. Louis, J. Phys. Chem. C 113 (2009) 2903.
[9] T. Oishi, T. Katayama, K. Yamaguchi, N. Mizuno, Chem. Eur. J. 15 (2009) 7539.
[10] T. Oishi, K. Yamaguchi, N. Mizuno, ACS Catal. 1 (2011) 1351.
[11] K. Sonogashira, in: E. Negishi (Ed.), Handbook of Organopalladium Chemistry for Organic Synthesis, Wiley, New York, 2002, p. 493.
[12] K. Sonogashira, J. Organomet. Chem. 653 (2002) 46.
[13] C. Gonzalez-Arellano, A. Abad, A. Corma, H. Garcıa, M. Iglesias, F. Sanchez, Angew. Chem. Int. Ed. 46 (2007) 1536.
[14] S.K. Beaumont, G. Kyriakou, R.A. Lambert, J. Am. Chem. Soc. 132 (2010) 12246.
[15] M. Boronat, D. Combita, P. Concepción, A. Corma, H. García, R. Juárez, S. Laursen, J.D. Lopez-Castro, J. Phys. Chem. C 116 (2012) 24855.
[16] J.P. Perdew, J.A. Chevary, S.H. Vosko, K.A. Jackson, M.R. Pederson, D.J. Singh, C. Fiolhais, Phys. Rev. B 48 (1993) 4978.
[17] J.P. Perdew, Y. Wang, Phys. Rev. B 45 (1992) 13244.
[18] G. Kresse, J. Furthmüller, Phys. Rev. B 54 (1996) 11169.
[19] G. Kresse, J. Hafner, Phys. Rev. B 47 (1993) 558.
[20] P.E. Blöchl, Phys. Rev. B 50 (1994) 17953.
[21] A. Heyden, A.T. Bell, F.J. Keil, J. Chem. Phys. 123 (2005) 224101.
[22] G. Henkelman, H. Jónsson, J. Chem. Phys. 111 (1999) 7010.
[23] G. Henkelman, H. Jónsson, J. Chem. Phys. 113 (2000) 9978.
[24] E. Sanville, S.D. Kenny, R. Smith, G. Henkelman, J. Compos. Chem. 28 (2007) 899.
[25] G. Henkelman, A. Arnaldsson, H. Jónsson, Comput. Mater. Sci. 36 (2006) 254.
[26] C. Loschen, J. Carrasco, K.M. Neyman, F. Illas, Phys. Rev. B. 75 (2007) 035115.
[27] L. Alves, B. Ballesteros, M. Boronat, J.R. Cabrero-Antonino, P. Concepción, A. Corma, M.A. Correa-Duarte, E. Mendoza, J. Am. Chem. Soc. 133 (2011) 10251.
[28] J. Oliver-Meseguer, J.R. Cabrero-Antonino, I. Domínguez, A. Leyva-Pérez, A. Corma, Science 338 (2012) 1452.
[29] M. Boronat, A. Leyva-Pérez, A. Corma, Acc. Chem. Res. 47 (2014) 834.
[30] A. Roldán, S. González, J.M. Ricart, F. Illas, ChemPhysChem 10 (2009) 348.
[31] M. Boronat, A. Corma, Dalton Trans. 9 (2010) 8538.
[32] L.M. Molina, M.D. Rasmussen, B. Hammer, J. Chem. Phys. 120 (2004) 7673.
[33] I. Remediakis, N. Lopez, J. Norskov, Angew. Chem. Int. Ed. 44 (2005) 1824.
[34] J. Wang, B. Hammer, Phys. Rev. Lett. 97 (2006) 136107.
[35] I.X. Green, W. Tang, M. Neurock, J.T. Yates Jr., Science 333 (2011) 736.
[36] S. Laursen, S. Linic, J. Phys. Chem. C 113 (2009) 6689.
[37] S. Laursen, S. Linic, Phys. Chem. Chem. Phys. 11 (2009) 11006.
[38] S. Carrettin, M.C. Blanco, A. Corma, A.S.K. Hashmi, Adv. Synth. Catal. 348 (2006) 1283.
[39] J. Zheng, C. Zhang, R.M. Dickson, Phys. Rev. Lett. 93 (2004) 077402/1.
[40] J. Oliver-Meseguer, A. Leyva-Pérez, A. Corma, ChemCatChem 5 (2013) 3509.